Hindawi
Shock and Vibration
Volume 2023, Article ID 1528983, 17 pages
https://doi.org/10.1155/2023/1528983

Research Article

Study on Joint Damage of Double Prefabricated Fragments Penetrating Finite Thickness Concrete

Zhenning Wang,[1] Junhui Yang,[2] Jianping Yin ,[1] Xudong Li,[1] Rui Shi,[3] and Jianya Yi[1]

[1]*College of Mechanical and Electrical Engineering, North University of China, Taiyuan 030051, China*
[2]*Unit 63961 of PLA, Beijing 100012, China*
[3]*Systems Engineering Research Institute, Beijing 100081, China*

Correspondence should be addressed to Jianping Yin; yjp123@nuc.edu.cn

Received 23 July 2022; Revised 2 March 2023; Accepted 7 March 2023; Published 3 April 2023

Academic Editor: Sandro Carbonari

In order to study the joint damage mechanism of multiple prefabricated fragments to finite thickness concrete targets, experiments on the damaging effect of a single fragment on a 300 × 300 × 100 mm concrete target were carried out, and the reliability of the simulation calculation model of single fragment damage to concrete was verified. On this basis, according to the trajectory of two fragments penetrating concrete, the double fragment penetration is divided into two penetration situations, that is, coplanar and heterogeneous. The orthogonal optimization method is used to carry out the joint damage simulation calculation of the double fragments to the concrete target by changing the fragment velocity, penetration angle, fragment spacing, and other factors. The simulation results show that the relationship between joint damage and fragment spacing is the largest when the fragment trajectories are coplanar, and the partial least squares regression coefficients affecting the joint damage time and surface joint length are 0.70 and 0.68 respectively. When the trajectory is different, the joint damage mode is relatively complex. Based on this, the joint damage degree analysis method between fragments is established, and each variable can explain 73.8% of the joint damage degree. It is found that the joint damage of the front pit area is the largest when the fragment is in different planes, and the PLS regression coefficient is −0.44. The hypothesis that joint damage is easy to occur in the area of the intersection line on the back of the target is analyzed and verified.

1. Introduction

Fragment, as a damaged element, has natural fragments, semiprefabricated fragments, prefabricated fragments, and other types. Prefabricated fragments are used to make the fragments fly evenly and the damage range adjustable, so that the fragment damage element is controllable and the damage efficiency tends to be stable [1]. Due to the large number of fragments generated by the kill and explosion warhead, the fragments generated in the dynamic explosion state are more concentrated than those in the static explosion state. When fragments act on a target, using the penetration depth or damage effect of a single fragment as a basis for judgment is one-sided and cannot describe the damage to the target in a practical sense. Studying the joint damage of multiple fragments to the target can more comprehensively analyze the damage of the target.

Concrete is a common material for modern buildings and fortifications, and its excellent strength and plasticity have become the first choice for various man-made fortifications [2]. The large caliber penetrator, represented by the ground-penetrating projectile, usually deals with the large-thickness of concrete fortification [3], while the anti-explosive projectile has a good destructive effect on the concrete wall with finite thickness [4]. Thus, it is of practical significance to study the combined damage of multiple fragments to the concrete with finite thickness.

At present, a large number of experts and scholars have carried out various types of penetration tests on concrete, and the concrete model parameters in the simulation are

compared[5]. In reference [2], the experiment and numerical simulation of missile penetration into the reinforced concrete target plate are compared, and the simulation model can well describe the damage mechanism of the structure, and it also introduced the calculation method of low strength concrete penetration depth, and the calculation formula of the residual velocity was also introduced [6]. The damage characteristics of projectiles with different head shapes penetrating the concrete are studied, and the relationship between the back damage of the target plate and the shape of the warhead is analyzed [7]. The literature [8] analyzed the crater area of 500 m/s–1700 m/s projectile penetrating concrete and found that the crater volume was linear with the kinetic energy of fragments. The relationship between the residual velocity of the projectile and the steel content in the concrete was found, and the oblique penetration of the projectile into the target plate was studied [9].

In the experiment, the vertical penetration of the projectile into concrete is the main experimental method, and the ballistic gun is widely used as the fragment-launching tool in a large number of papers and experiments in the world, so that the fragment speed can achieve high speed and controllable range. Cheng et al. [10] studied the antipenetration performance of vertically penetrating concrete targets and obtained the effect of reinforcement ratio on the antipenetration performance of reinforced concrete. Deng and Chen [11] analyzed the vertical penetration of the projectile into the concrete target from the test and numerical simulation, obtained the damage zone of the concrete during the penetration process, and carried out in-depth research studies on the corresponding mechanical zone of the concrete under impact. For the oblique penetration of concrete, Liu et al. [12] conducted tests on the oblique penetration of reinforced concrete targets and obtained the equivalent method of reinforcement mesh. Shen et al. [13] tested the oblique penetration of the projectile into the concrete and analyzed the damage mode of the oblique penetration to the concrete. In addition, Duan et al. [14] analyzed the critical rebound of the projectile penetrating concrete, revealing the rebound phenomenon of the fragments under a large penetration angle. In the aspect of tungsten alloy projectile penetration, Zhou and Li [15] studied the ultrahigh speed penetration mechanism of concrete targets, found the relationship between penetration depth and velocity of the projectile, and compared various formulas. Considering the erosion and destruction of concrete, Liu et al. [16] analyzed the quality erosion model of concrete. On concrete materials, Lv et al. [17] studied the penetration mechanism of ultrahigh-performance concrete targets.

Among the equations describing concrete, the RHT equation of state is widely used to describe the damage of concrete [18, 19]. The RHT equation of state can directly display the characteristics of concrete cracking, damage degree, and so on, but it is not completely consistent with the actual damage comparison [20]. This is because the RHT state equation cannot completely correspond to the actual damage mode when describing the tensile strength and shear strength, and the concrete damage has a certain degree of randomness, so it is necessary to carry out appropriate parameter verification and use appropriate methods to visually describe its damage.

In practice, the dispersion mode of prefabricated fragments is relatively random, and the intersection path of the penetrating concrete is very complex. With the influence of the initial variables of prefabricated fragments, the damage forms and damage degrees of concrete walls will be varied. The purpose of this paper is to study the combined damage mode of multiple fragments to concrete walls. First, the damage mode of a single fragment impacting the concrete is analyzed by experiments. The purpose is to study the impact of initial conditions of combined penetration of fragments on the damage mode of concrete walls and discover the rules between them. Based on the damage characteristics of concrete walls in the single fragment penetration test, the numerical simulation study of the damage of two fragments to concrete under multivariable conditions is carried out.

2. Materials and Methods

There are a large number of fragments in the prefabricated fragment bomb. Considering the simplest mode, the damage of multiple fragments can be simplified to the damage between any two damaged elements, and then the criterion of joint damage of double fragments is applied to the damage of the whole target. The fragments of a single explosive bomb scatter regularly, and the motion trajectories of the fragments are approximately parallel. When multiple explosive bombs act on the same target, the initial variables between fragments do not affect each other, so it is necessary to study the possible damage.

The prefabricated fragment material is tungsten alloy, and the target plate material is concrete. Johnson Cook equation of state is selected for tungsten alloy, and the parameters of tungsten alloy material are shown in Table 1. The RHT equation of state is selected for the target plate, and the parameters of RHT material are shown in Table 2. Erosion contact is applied to RHT material [21] to avoid large grid deformation during penetration, and the concrete damage area can be seen intuitively. In order to simulate various types of joint damage forms, the wall thickness is selected as 80 mm (the wall thickness of buildings is generally more than 50 mm) and boundary constraints are imposed around the concrete target to limit its displacement.

Figure 1 shows the simulation model of penetration into concrete when the fragment trajectories are coplanar. When the two fragment trajectories are basically parallel, the initial variables are regarded as the same. Perform a four-variable three-level orthogonal optimization design for the parameters of the fragment, and the orthogonal optimization is shown in Table 3.

2.1. Modeling of Fragment Trajectory in Different Surface Penetration. In order to fully consider the joint damage of two fragments, the experimental personnel combined the possible penetration modes of any two fragments. The method is to make the two fragments independent of each other, take the plane of the normal vector of the target plate

Table 1: Tungsten alloy material parameters.

Material	R_0	E	PR	SIGY	BETA
Tungsten alloy	$1.8167E^{-5}$	344.7	145	1.87	1.0

Table 2: RHT equation of state parameters.

R_0	*Shear*	*EPSF*	B_0	B_1	T_1
$2.7e^{-6}$	26.7	2	1.22	1.22	100
F_C	F_S	F_T	Q_0	B	T_2
0.035	0.18	0.1	0.6805	0.0105	0.0

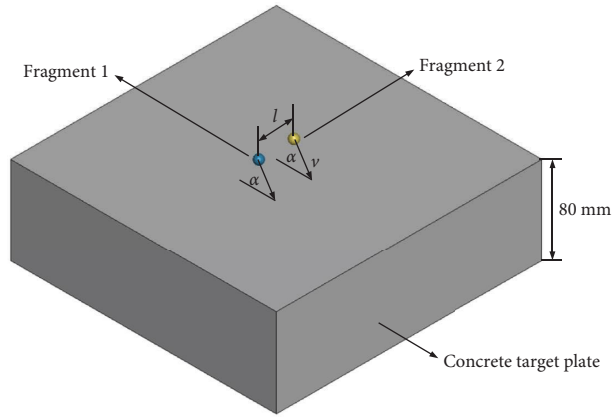

Figure 1: Modeling of double fragment penetration in coplanar.

Table 3: Coplanar double fragment orthogonal optimization of four variable three-level variables.

Number	Fragment diameter d (mm)	Fragment velocity v (m/s)	Incident angle α (°)	Fragment spacing l (mm)
1	6	1000	0	20
2	8	1500	15	30
3	10	2000	30	40

passing through the falling point of the fragments as the trajectory plane of the fragments, determine the velocity and direction of each fragment in the respective trajectory plane according to the trajectory plane of the two fragments, and then obtain the possible combination between any two fragments.

According to the intersection process shown in Figure 2, after determining the distance between the landing points of the two fragments, fix the fragment 1 and the penetration surface to determine the position of the fragment 2 and the penetration surface. A horizontal analysis was conducted for five variables (landing point d, penetration trajectory plane included angle α, angle between fragment 1 and normal vector $\beta 1$, angle between fragment 2 and normal vector $\beta 2$, and the speed combination of fragments), and the orthogonal optimization design is shown in Table 4. In order to achieve the purpose of joint damage research studies, the range of the included angle α of the penetration trajectory plane should be determined within the range of 0~90° to ensure the intersection of the damaged areas of the two fragments. The angle between the two fragments and the normal vector is selected as 0~60° to avoid fragment bouncing.

2.2. Comparison between Test and Simulation of Fragment Penetrating Concrete. The 12.7 mm ballistic gun is used in the fragment penetration concrete test, and the concrete block is placed in the target box. The target plate parameter is $300 \times 300 \times 100$ mm, and two velocity-measuring targets are set in front of and behind the target box and connected with a six-channel velocimeter to measure the initial velocity and residual velocity of fragments. Figures 3 and 4 show the schematic diagram and physical diagram of a fragment penetration test.

The abovementioned device is used to test the ballistic gun of 11 mm tungsten alloy spherical fragments. In Figure 4, a is the fragment, sabot, and cartridge, and ① in b is the front velocity target; ② is the rear tachometer target; ③ is the target box for placing concrete; ④ is the wire

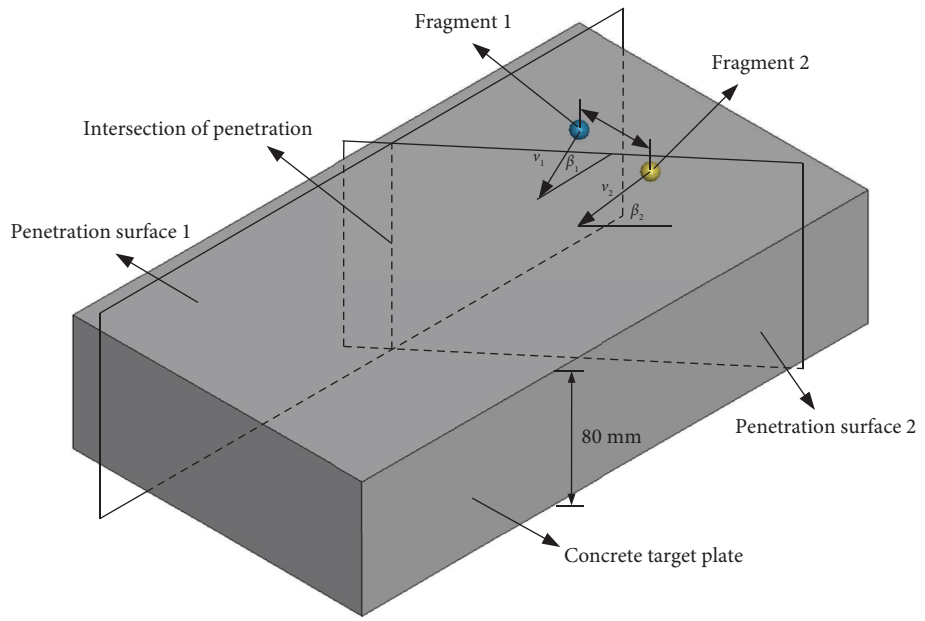

Figure 2: Modeling of double fragment penetration in different planes.

Table 4: Orthogonal optimization table of 5 factors and 5 levels for different surface fragment penetration.

Numbers	d (mm)	α (°)	β_1 (°)	β_2 (°)	Combinations (m/s)	
					v_1	v_2
1	20	15	0	0	500	1000
2	30	30	15	15	500	2000
3	40	45	30	30	1000	1000
4	50	60	45	45	1000	2000
5	60	75	60	60	2000	2000

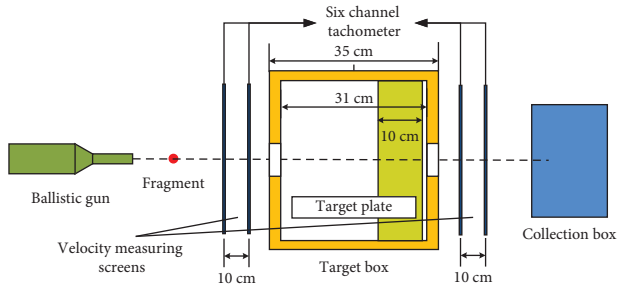

Figure 3: Schematic diagram of a test plan.

connecting the tachometer. The experiment controlled the amount of charge in the cartridge to achieve different initial velocities for the fragments.

The penetration test of tungsten alloy fragments into concrete was carried out 6 times in the speed range of 752 m/s~1463 m/s. Table 5 shows the initial speed, residual speed, and simulated residual speed of fragments.

Figures 5 and 6 show the damage to the front and back of the target plate with fragment velocities of 974 m/s and 1166 m/s. From the damaged form of concrete, it can be seen that the front and back of the target plate are truncated cone-shaped pit areas, the damage degree of the back is larger than that of the front, and the middle is a channel slightly larger than the diameter of the fragment. Due to the small size of the target plate, the crack extends around, making the target plate crack along the path closest to the boundary. In order to analyze the damage of the target plate in the front pit, rear pit, and tunnel area, the length and width parameters and characteristics of the three areas of the target plate are measured, as shown in Table 6.

From Table 6, it can be seen that the maximum difference between the rear pit and the simulation in the test is 19.6%, the maximum difference between the front pit diameter and the simulation is 17.6%, and the maximum difference between the tunnel area and the simulation is 16.4%. The main reason for the small analysis simulation

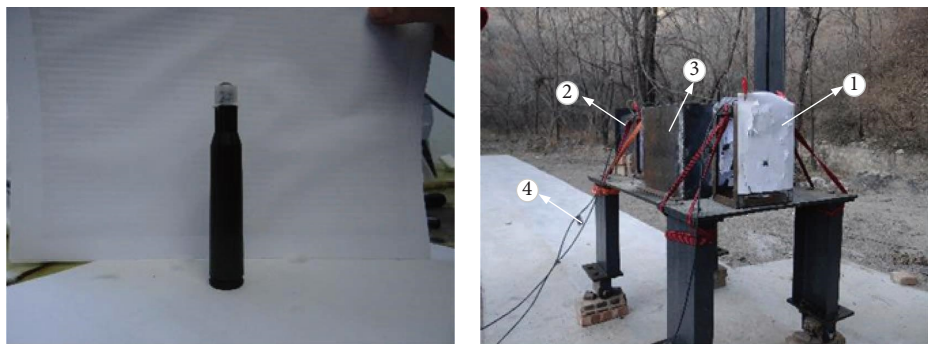

(a) (b)

Figure 4: Physical diagram of a test device.

Table 5: Test conditions.

Number	Target type	Initial speed (m/s)	Residual speed (m/s)	Simulation residual speed (m/s)
1	100 mm thick	752.74	64.40	35.35
2	100 mm thick	974.71	94.17	135.87
3	100 mm thick	1166.05	22.54	153.68
4	100 mm thick	1462.96	378.40	326.54
5	100 mm thick	1247.46	115.78	187.46
6	100 mm thick	1322.18	301.80	268.75

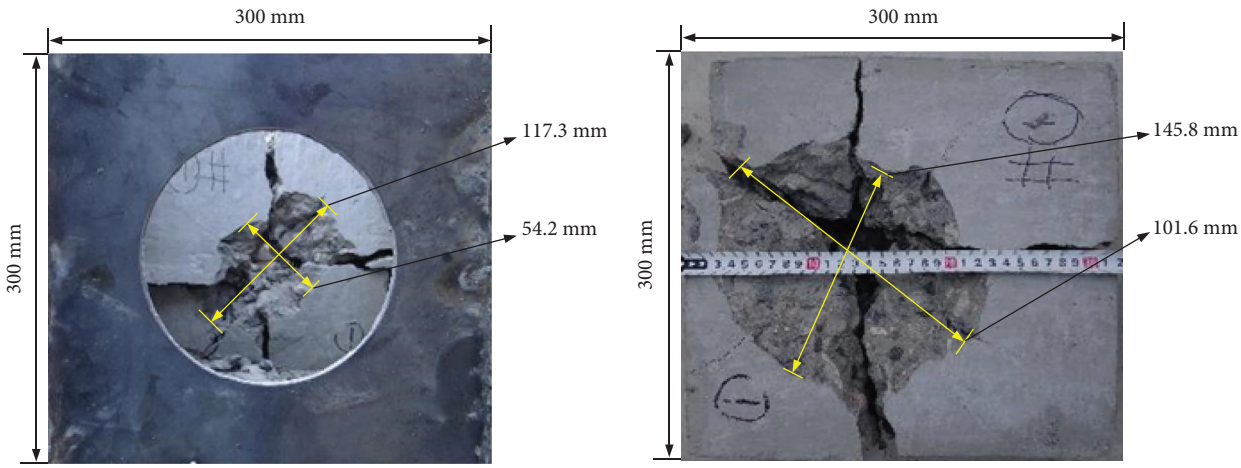

(a) (b)

Figure 5: Front and back of target plate damage with a fragment velocity of 974 m/s.

value is that there is a part of the target surface collapse area in the front and rear pit areas, and the back collapse is more obvious. The depth of this part of the area along the vertical direction of the target surface is small, which has a very small impact on the main strength of the concrete target plate. In the simulation, the RHT model cannot simulate the microavalanche effect at the edge of the front and rear pits on the target surface, so the simulation value is less than the experimental value.

As shown in Figure 7, the simulation and experimental results with a fragment velocity of 1166 m/s are compared. From the simulation results, it can be seen that the RHT model can better simulate the main failure forms of the three zones of concrete front pit, tunnel, and rear pit and can observe the crack of the target plate from the damage cloud diagram of damage, which is consistent with the crack extension of tungsten alloy fragments on finite thickness concrete in the experiment. When fragments penetrate the concrete, three areas as shown in Figure 8 will generally be generated. Different types of concrete damage forms can be obtained by combining and analyzing the damage conditions of different types of target plates.

When the trajectories of the two fragments are coplanar, the joint action between the fragments is relatively

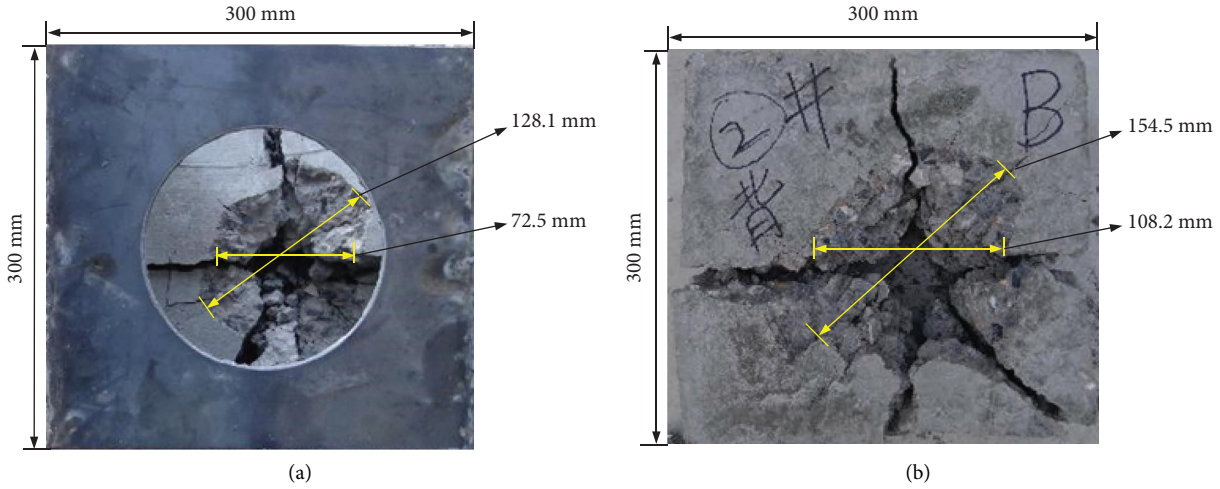

Figure 6: Front and back of target plate damage with a fragment velocity of 1166 m/s.

Table 6: Comparison of damage data between the test and simulation target.

Number	Velocity v (m/s)	Maximum diameter of the front pit (mm)	Minimum diameter of the front pit (mm)	Average diameter of the front pit (mm)	Maximum diameter of the rear pit (mm)	Minimum diameter of the rear pit (mm)	Average diameter of the rear pit (mm)	Tunnel diameter (mm)
Test	974	117.3	54.2	85.75	145.8	101.6	123.7	16.3
Simulation	974	—	—	75.8	—	—	101.8	14.1
Test	1166	128.1	72.5	100.30	154.5	108.2	131.35	19.4
Simulation	1166	—	—	82.6	—	—	105.6	16.2

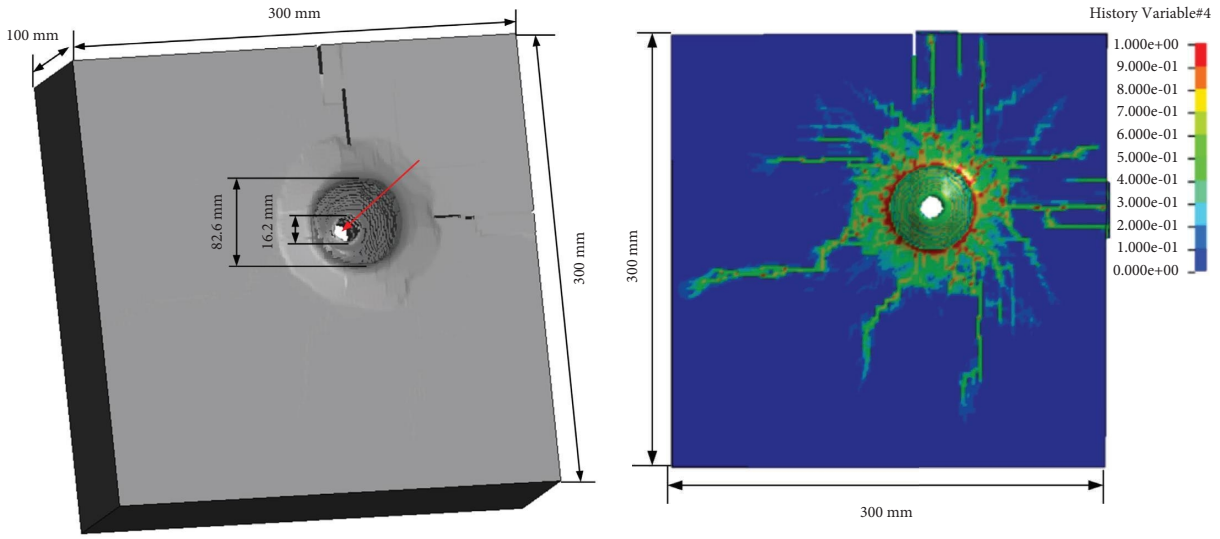

Figure 7: Simulation results of a fragment velocity of 1166 m/s.

continuous. The nearly parallel penetration mode of the two fragments makes the damage of the two fragments to the concrete always in the joint state. Under the combined action of the two fragment stresses, the concrete between the two fragments is superimposed by the stresses of the two fragments, which increases the damage degree of the concrete between the two fragments.

When the trajectories of the two fragments are different, the initial conditions of the two fragments are not related to each other. As is shown in Figure 9, the two fragments' area

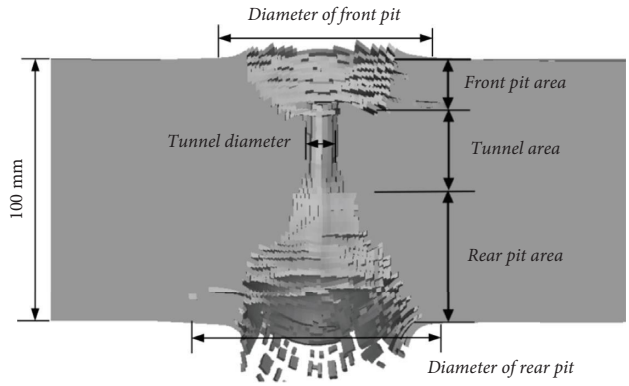

Figure 8: Damage zone when fragments penetrate the concrete.

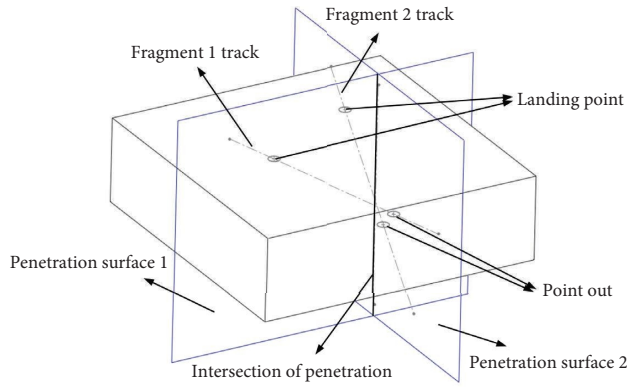

Figure 9: Schematic diagram of the assumption that joint damage occurs in the intersection area of the penetration surface.

response to the superposition on the back of the concrete target may be near the intersection line of the plane where the two fragments are located. Therefore, it is speculated that this area is more prone to joint damage.

The following is a joint damage analysis of double fragments based on experiments, simulations, and theoretical assumptions.

2.3. Combined Damage of Double Fragments to Concrete. Because of its small size and fast speed, the damage mode of fragments penetrating thin concrete target plates is relatively complex. When the fragment mass is too small or the penetration angle is too large, fragments may be embedded into the target plate. When the damaged areas of two fragments overlap, there will be a joint effect between them, and the damaged areas cannot be analyzed separately.

2.3.1. Impact of Penetration Angle on Concrete Damage. Because the initial conditions of fragments in coplanar penetration are relatively consistent, the damaged form of fragments is studied in the same way as that of the single fragments. The main influencing factors here are fragment velocity and penetration angle. First, the difference between forward penetration and oblique penetration in the case of a single fragment is analyzed and the main characteristic difference between normal penetration and oblique penetration occurs in the open pit area and the collapse area.

Table 7 shows the concrete strain nephogram of a single fragment penetrating concrete at the same speed and different angles. By comparing the penetration trajectories of 0°, 10°, 20°, 30°, 40°, 50°, and 60°, we can see the differences in concrete damage. Here, the finite-thickness concrete target plate is 100 mm, and the fragment velocity is 2000 m/s, and the RHT concrete model that has been tested and compared is adopted. The purpose here is to provide a preliminary reference for the orthogonal optimization numerical simulation of multiple penetration velocities and angles and to find the difference in concrete damage through the penetration trajectory under different penetration angles. From Table 7, it can be seen that the change in penetration angle affects the trajectory length of fragments and changes the front and back of the target plate concrete damage form of the intermediate track.

The collapse area is similar to the pit opening area. Except for the damaged area near the fragment flying-out point, the collapse effect will also occur under the fragment trajectory, presenting an irregular truncated cone-damaged area. Compared with the two, the tunnel area is relatively stable, and the diameter of the tunnel area changes little except for the starting and ending positions of the tunnel area.

2.3.2. Coplanar Joint Damage. Table 8 shows the joint damage process of the cross-section during coplanar penetration. As the penetration depth of fragments increases, the damaged strain region of the concrete also expands. The expansion of the damaged area lags behind the fragment penetration process, and the damage degree of the area between fragments gradually increases and becomes invalid. From the front of the target plate, the commonly damaged part presents an elliptical damaged area. Then, several parameters of the front pit area are used to analyze the joint damage.

Figure 10 shows the two analysis objects in the first group of orthogonal optimization (when the fragment trajectories are parallel). The left side of Figure 10 is the first object parameter studied in this paper, that is, the boundary connection length of the two fragments to the concrete damage, which indicates the effect of the combined penetration of the two fragments on the concrete impact surface after the concrete penetration. On the right side of the figure is the second parameter studied in this paper, that is, the occurrence time of the combination of the strain area of the two fragments to the concrete damage, which describes the experience time when the two fragments just contact from the beginning of the penetration to the boundary of the strain area. This parameter indicates that the initial variables of the fragments have an impact on the starting time of the joint penetration, which to a certain extent determines the size of the joint damage of the two fragments to the concrete.

Table 7: Comparison of strain nephogram of oblique penetration at different angles.

Angle	0.02 ms	0.07 ms	0.22 ms	0.52 ms	Ruler
0°	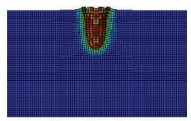	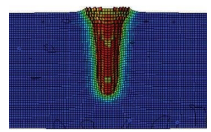	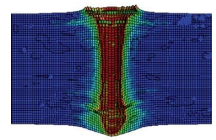	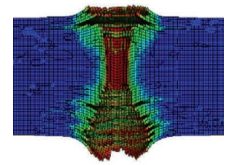	 80 mm
10°	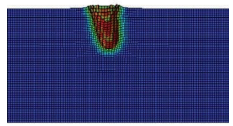	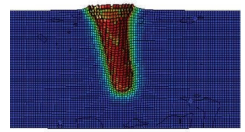	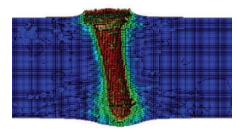	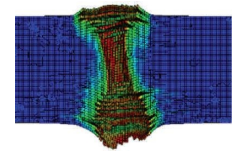	 80 mm
20°	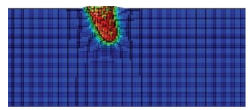	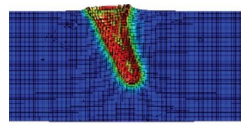	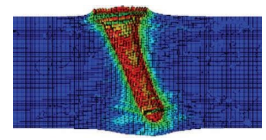	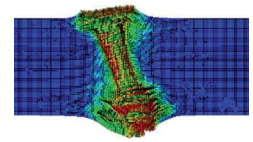	 80 mm
30°	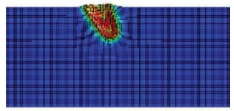	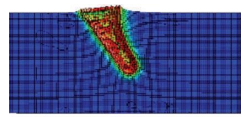	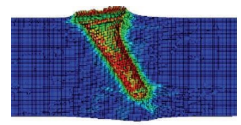	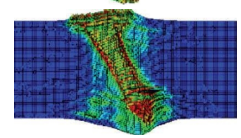	 80 mm
40°	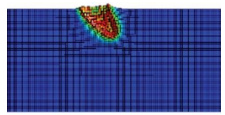	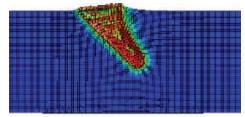	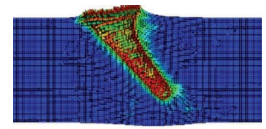	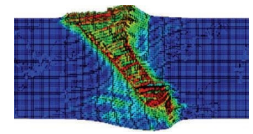	 80 mm
50°	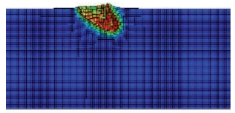	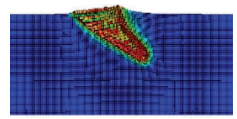	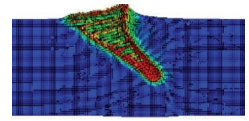	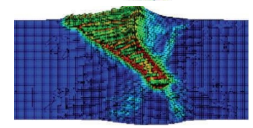	 80 mm
60°	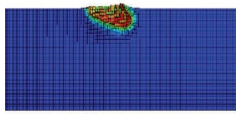	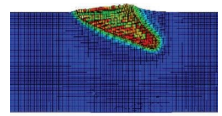	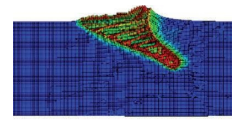	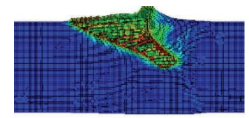	 80 mm

Table 8: Joint damage process of coplanar penetration.

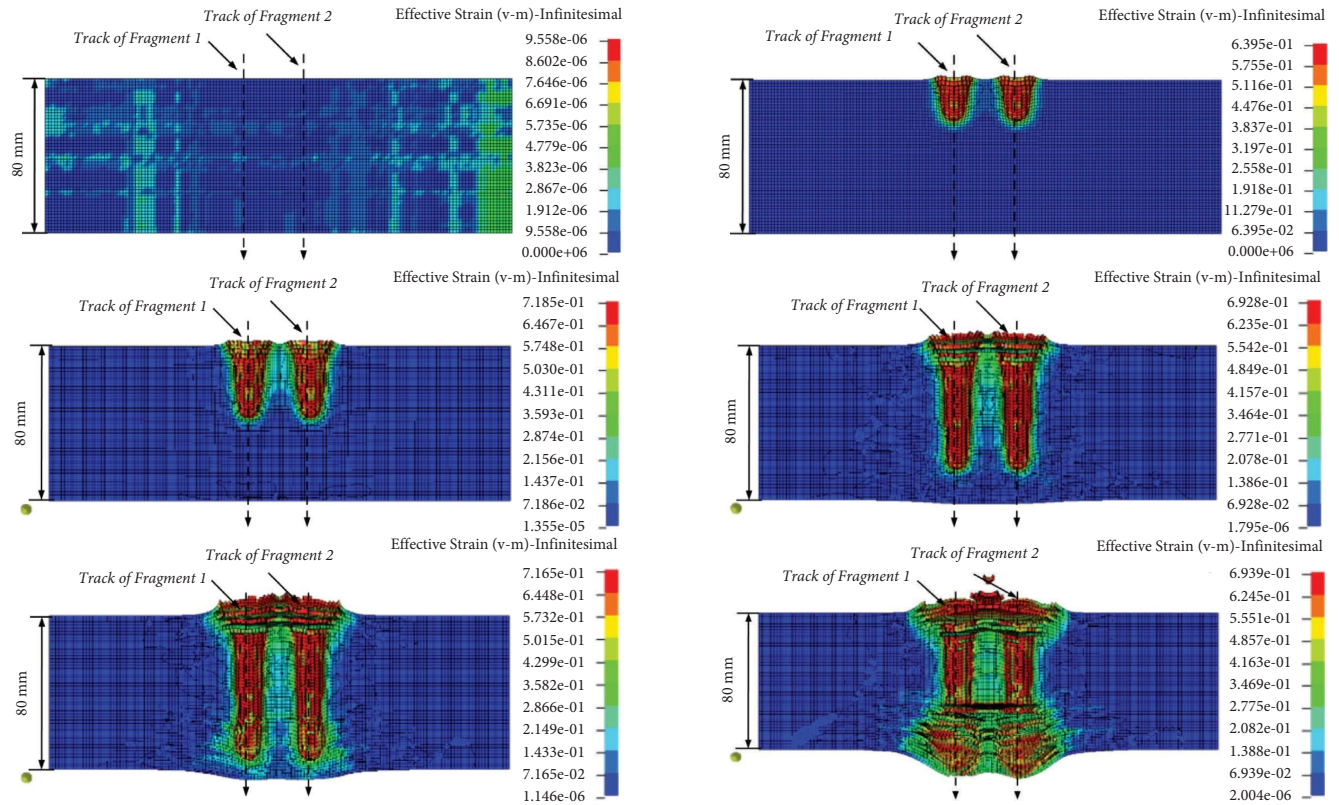

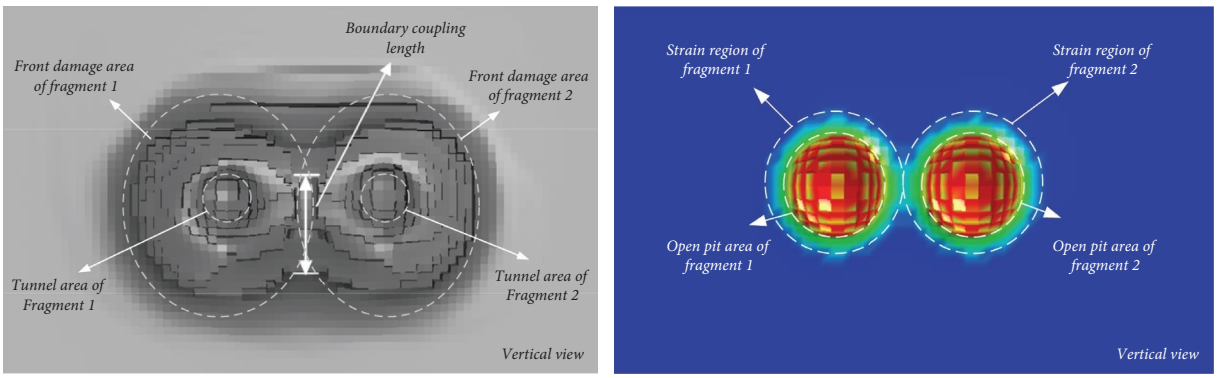

Figure 10: Surface joint length and surface joint occurrence time.

Table 9 shows several joint damage parameters of the concrete excavation area. The joint length of the boundary is the length of the boundary of the two fragments, and the greater the value, the greater the degree of joint damage. The surface joint time is the time when the strain region first meets in the strain cloud diagram. The smaller the time is, the earlier the joint starts. According to the data obtained from the coplanar damage process and results, the range analysis of the joint occurrence time of the double fragment surface and the joint length of the final surface boundary is carried out in turn.

Figure 11 shows the mean value of the influence of various factors on the occurrence time of surface joints. The significance of this numerical discussion is the initial response time of the front joint damage of the target plate when the fragment trajectory is coplanar, and this determines the impact of fragment diameter, fragment velocity, tilt angle, and fragment spacing on the response time. The three variables, fragment velocity, tilt angle, and fragment spacing, present a monotonic trend. The greater the velocity, the shorter the time for joint occurrence, and the greater the tilt angle and spacing, the longer the time for

Table 9: Results of coplanar double fragment penetration into the open pit area.

Number	Surface joint occurrence time (ms)	Boundary joint length (mm)	Length of pit opening area (mm)	Width of pit opening area (mm)
1	0.015	33	49.5	33
2	0.025	33.55	68.8	40.15
3	0.04	28.6	79	40.8
4	0.11	16.5	77.4	32.64
5	0.01	43	65.36	43
6	0.02	38.7	77.4	44.2
7	0.02	36.96	71.4	38.64
8	0.035	34	81.6	40.8
9	0.007	67.94	69.66	67.94

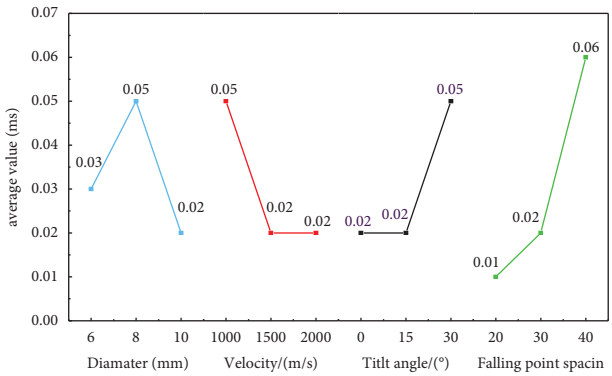

Figure 11: Influence of various factors on the occurrence time of surface association.

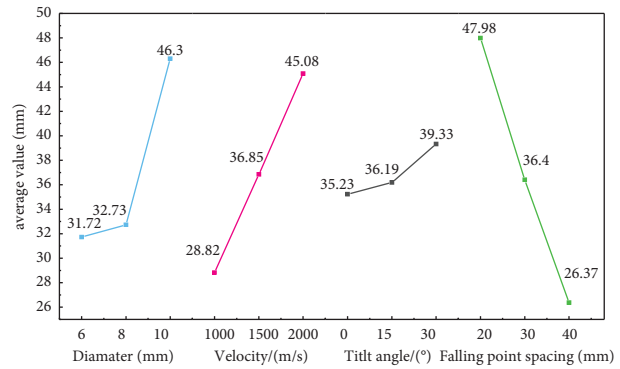

Figure 12: Influence of various factors on the occurrence time of surface association.

joint occurrence. At this moment, fragment spacing has the greatest impact.

As shown in Figure 12, the influence of various factors on the joint length of the front face is shown. On the basis of the response time of the front face of the target plate, the influence of four variables, namely, fragment diameter, fragment velocity, tilt angle, and fragment spacing, on the joint damage is discussed. The four variables of fragment diameter, fragment velocity, tilt angle, and fragment spacing all present a monotonic trend. The larger the diameter, velocity, and tilt angle are, the larger the joint length of the surface is, while the larger the fragment spacing is, the smaller the joint length is. There is also a case where the fragment spacing has the greatest impact.

In order to study the influence of the abovementioned four variables on the specific size of the abovementioned two parameters, the positive and negative influence rules of each variable on the two parameters are obtained. As shown in Figure 13, PLS regression analysis is carried out for the joint occurrence time of the surface and the joint length of the boundary. Through this regression analysis, the positive and negative effects of each dependent variable on the results can be obtained. It can be seen that fragment spacing has the greatest impact on joint damage, followed by fragment speed. Although the large inclination angle affects the occurrence time of the joint, it has a small impact on the final joint length of the boundary, and the fragment speed and fragment spacing have a significant impact on the final joint damage.

2.3.3. Analysis of Combined Damage of Different Planes. When the fragment trajectory is different, the damaged areas of the joint damage area are staggered and complex at this time. The complex intersection mode causes the joint damage of the two fragments at different positions in the concrete, resulting in different failure forms of the open pit area, tunnel area, and collapse area. Figure 14 will analyze the front pit area, tunnel area, and rear pit area, respectively.

The damage of the impact surface of the target plate is the joint damage between the front pit area of the two fragments, which is mainly related to the spacing of the fragments, followed by the joint damage near the trajectory intersection area caused by the velocity direction of the fragments. When the trajectory is different, the spacing and incident angle of the two fragments have a great impact on the damage of the impact surface. The spacing affects the size of the joint damage by controlling the distance between the damage centers of the two fragments of concrete, and the incident angle affects the damage direction of the elliptical area in the open pit area. Figure 14 shows the damage form that only occurred on the front of the impact. Through this strain nephogram, we can see the joint process of the penetration of two fragments. At this time, the larger the incident angle of fragments is, the larger the damage area caused on the impact surface is.

Figure 15 shows the joint damage in the tunnel area, and the fragment spacing has the smallest impact on the concrete tunnel area among the damage of the three areas. The diameter of the tunnel area is slightly larger than the fragment

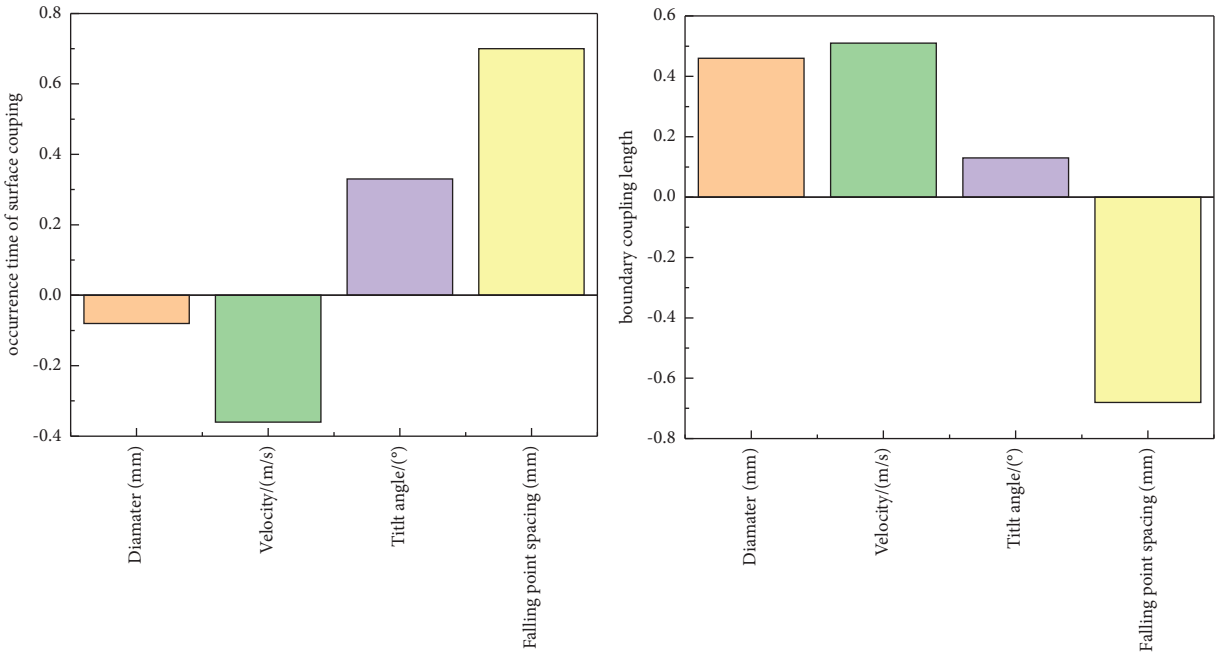

Figure 13: Normalized regression coefficient of surface joint occurrence time and boundary joint length.

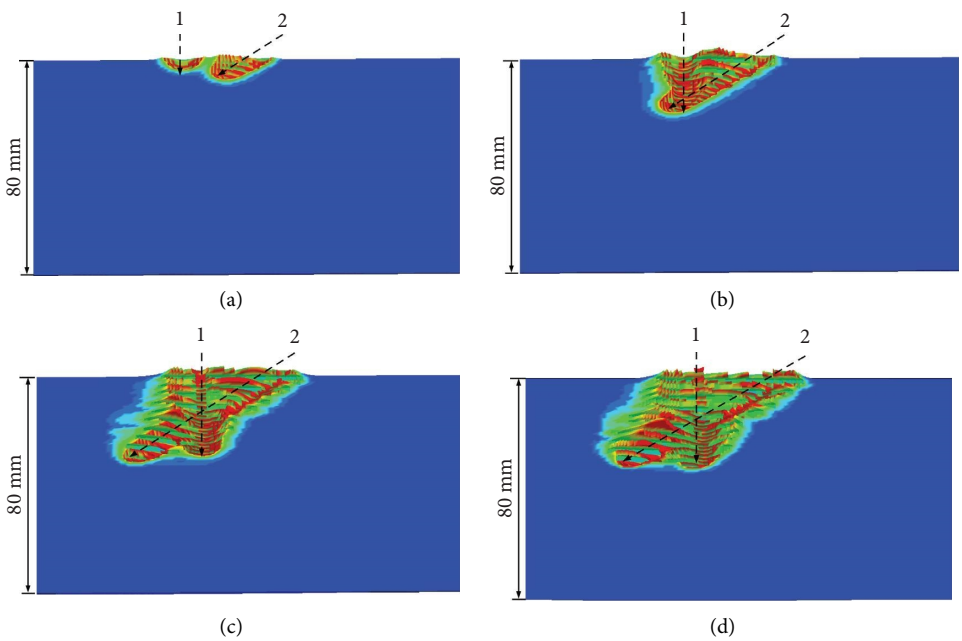

Figure 14: Cloud diagram of joint damage strain process of impact front. (a) 0.025 ms. (b) 0.075 ms. (c) 0.225 ms. (d) 0.375 ms.

diameter, and its length will change due to the influence of the inclination angle and velocity. Because it is less affected by other factors, unless there is a superposition of the tunnel areas, the degree of joint damage is small, which mainly depends on the distance between the tracks of the fragment tunnel areas.

The impact back is the possible area of collapse and damage in the direct penetration area. Figure 16 shows the joint damage process of the impact back. Since the damage degree of the back area is generally greater than that of the front when penetrating the concrete, the area of joint damage also increases correspondingly. The impact back is similar to the impact front, which is mainly affected by the distance between the penetration points on the back and the incident angle. The fragment velocity determines whether the fragment can reach this area. It can be seen from the abovementioned paragraph that the damage form of the collapse area is basically the damage of the truncated

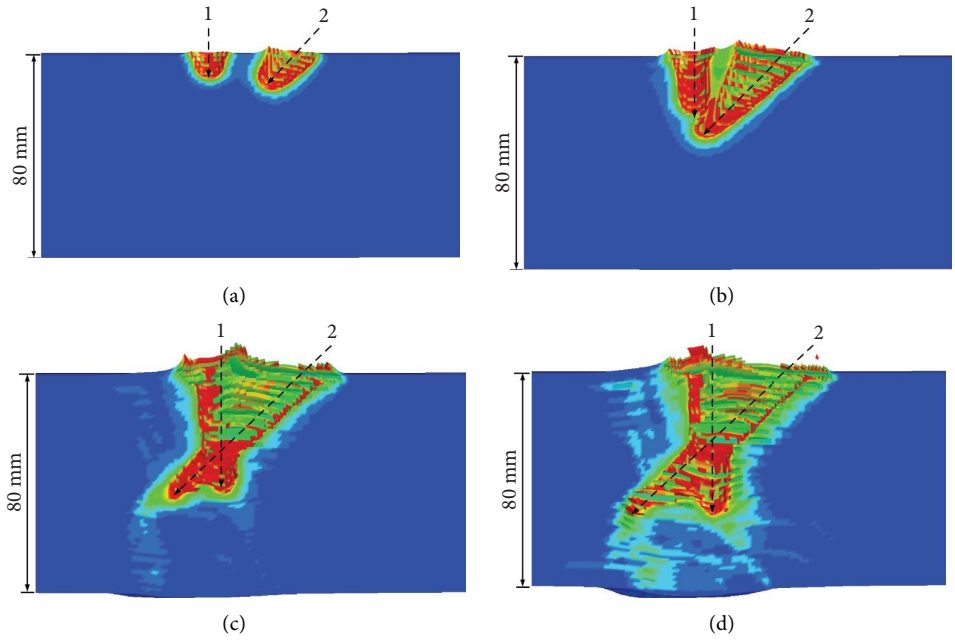

Figure 15: Cloud chart of joint damage strain process in the tunnel area. (a) 0.025 ms. (b) 0.075 ms. (c) 0.225 ms. (d) 0.375 ms.

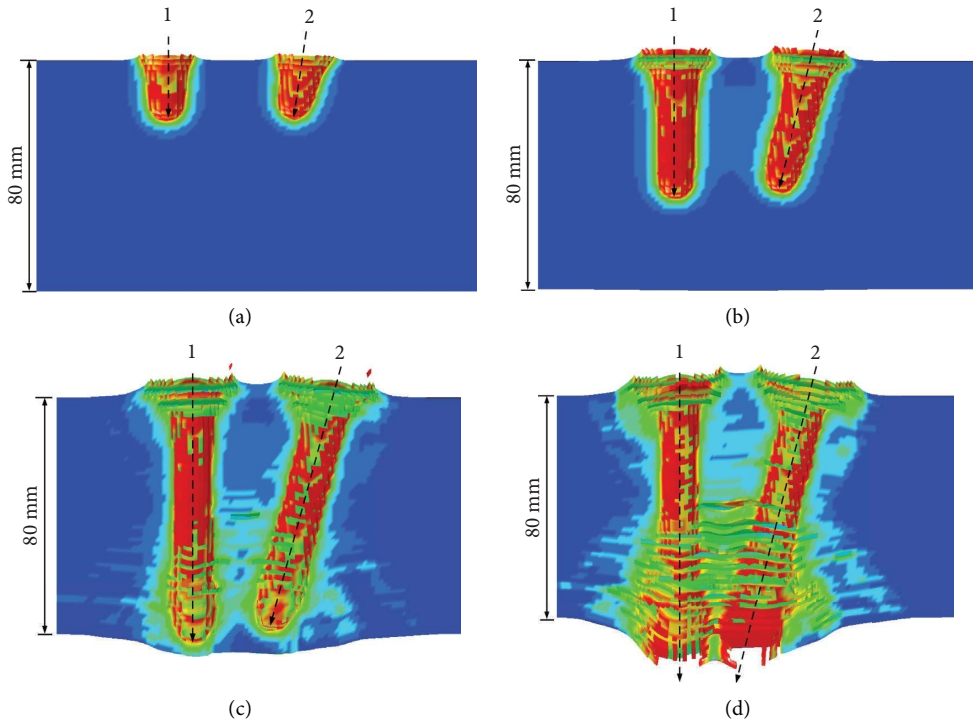

Figure 16: Cloud chart of joint damage strain process in the tunnel area. (a) 0.025 ms. (b) 0.075 ms. (c) 0.225 ms. (d) 0.375 ms.

cone-shaped area. The distance between the center point of the truncated cone and the fragment ejection point is affected by the angle, and the damaged area tends to shift to the bottom of the fragment trajectory. The combined damage of the front or back of the impact will reduce the tunnel area.

Taking the maximum damage surface of the two fragment tracks as the main view surface, six typical damage forms under different surface conditions are obtained in Figure 17.

To sum up, when studying the joint damage under the condition of different planes, the occurrence of joint damage

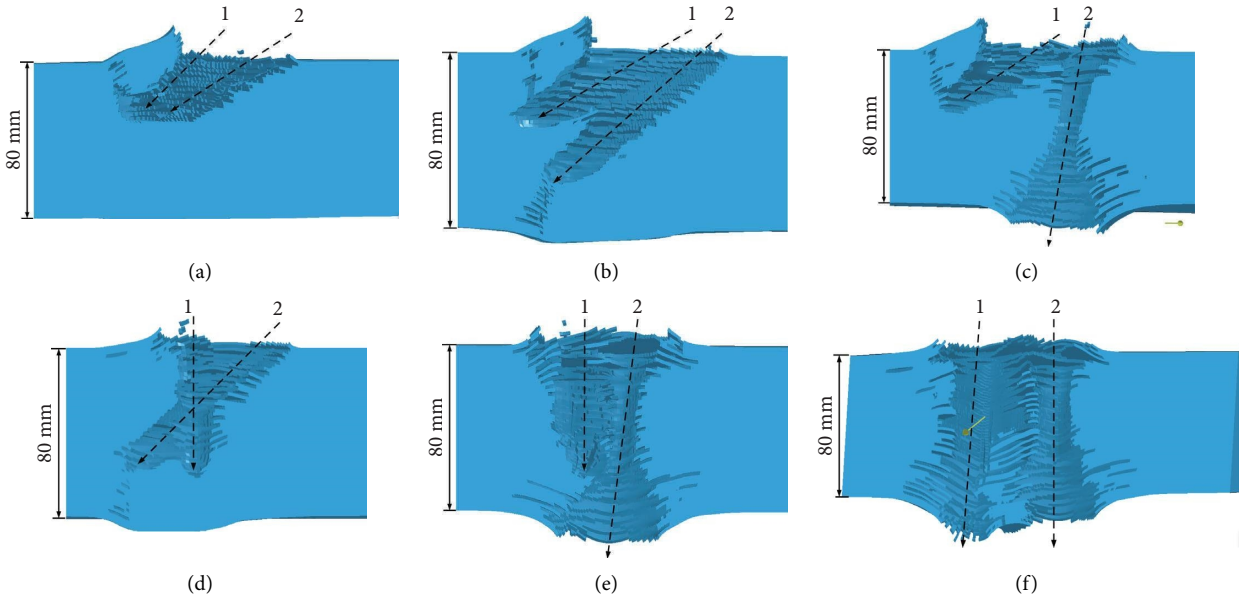

Figure 17: Typical six types of abnormal surface damage forms. (a) Front pit-front pit (group 8). (b) Front pit-tunnel (group 6). (c) Front pit-penetration (group 3). (d) Tunnel-tunnel (group 15). (e) Tunnel-penetration (group 7). (f) Penetration-penetration (group 11).

is taken as the evaluation basis, the combination of the three parts of the excavation area, tunnel area, and collapse area is taken as the evaluation condition, and the number of joint damage areas in each group is taken as the result of orthogonal optimization. 0 means that there is no union; 1 represents 1 position; 2 represents 2 positions; 3 represents three locations; and 25 groups of orthogonal optimization are divided into four joint damage degrees: 0, 1, 2, and 3. Table 10 shows the data statistics and joint degree of different surface damages.

Orthogonal optimization was carried out on the joint degree of concrete with two fragments, respectively. The results showed that there was no obvious rule for each variable, either for the overall joint degree or for the range analysis of the joint degree excluding the pit area. The orthogonal optimization variables and damage degree were analyzed by multifactor variance analysis. Table 11 shows the results of the multifactor variance analysis of the overall joint damage degree, and Table 12 shows the multifactor variance analysis of the joint damage degree excluding the open pit area.

It can be seen from the abovementioned multifactor variance results that each factor and level value of orthogonal optimization have a high degree of interpretation for the results of damage degree, and five variables can explain 73.8% and 76.3% of the parameters of damage degree.

From the damage of the concrete target, the impact point spacing in coplanar damage has a great impact on joint damage, and the influencing factors of joint damage are more affected by the distance between the fragment trajectories. According to the previous assumptions, the distance between the impact points and the average distance between the two fragments and the intersection line of the penetration surface can replace the angle between the penetration surface and the inclination of the two fragments. The combination of the distance between the impact points, the average distance between the penetration surface, and the velocity of the fragments can be used as variables to study the degree of damage using the PLS regression analysis method. The analysis results are shown in Figure 18.

From the final regression coefficient of the damage degree, it can be seen that the velocity combination has a positive impact on the damage degree of fragments, while the intersection distance and impact point spacing have a negative impact. When analyzing the damage degree of the concrete target as a whole, the impact point spacing plays a leading role, which confirms that the joint damage occurs most frequently in the open pit area in the 25 groups of orthogonal optimization simulation. After removing the joint damage in the open pit area, the intersection distance occupies the dominant position and the negative impact of exceeding the landing point spacing on the joint damage. That is, the greater the distance between the two fragments flying-out point and the intersection line, the smaller the joint degree of concrete.

2.4. Difference of Joint Damage of Two Fragments under Different Penetration Modes. From the joint damage analysis of the abovementioned two angles, there are great differences in the damage forms between coplanar and heterogeneous damage. Because the velocity vectors between fragments produced by coplanar damage are similar, the randomness of variables between them is small during penetration, and they are only affected by the penetration density of the fragments. The form of joint damage of coplanar penetration is relatively simple, and the destructive force of joint damage is greater than that of the coplanar penetration. The conditions for joint damage of different planes are relatively harsh, and usually they must fall at

Table 10: Orthogonal optimization of joint damage location and joint degree of each group.

Number	Joint damage location	Falling point spacing	Distance from the flying-out point to the intersection line (fragment 1)	Distance from the flying-out point to the intersection line (fragment 2)	Degree of association (overall)	Degree of association (remove pit opening)
1	Front pit + tunnel	20	5.36	20.7	2	1
2	Front pit + tunnel + penetration	20	−34.65	−56.9	3	2
3	Front pit	20	−118.56	6.86	1	0
4	Front pit	20	13.2	−98.56	1	0
5	Front pit	20	−5.36	31.1	1	0
6	Front pit	30	−130.52	−48.94	1	0
7	Front pit + tunnel	30	−4.12	13.2	2	1
8	Front pit	30	−50	−96.13	1	0
9	Front pit + tunnel + penetration	30	51.96	13.8	3	2
10	Front pit	30	65.8	115.9	1	0
11	Front pit + tunnel	40	−69.28	19.96	2	1
12	Front pit	40	23.1	−92.36	1	0
13	Front pit + tunnel + penetration	40	−6.2	10.37	3	2
14	No	40	−69.26	80	0	0
15	Front pit + tunnel	40	127.86	74.5	2	1
16	No	50	−32.8	−86.8	0	0
17	No	50	−109.69	11.5	0	0
18	Penetration	50	28.56	70.7	1	1
19	Front pit + tunnel + penetration	50	6.6	20	3	2
20	Penetration	50	186.6	171.76	1	1
21	No	60	−5.34	15.9	0	0
22	No	60	−45.36	69.3	0	0
23	No	60	60	4.85	0	0
24	No	60	57.7	98.56	0	0
25	Front pit	60	85.34	93.24	1	0

Table 11: Results of multifactor ANOVA of overall combined damage.

	Sum of squares	df	Mean square	F	p value
Intercept	36	1	36	21.176	0.010*
Falling point spacing	7.6	4	1.9	1.118	0.458
Angle of penetration surface	0.4	4	0.1	0.059	0.991
Fragment 1 angle	2.4	4	0.6	0.353	0.831
Fragment 2 angle	3.6	4	0.9	0.529	0.723
Speed combination	5.2	4	1.3	0.765	0.599
Residual	6.8	4	1.7		
		$R^2 = 0.738$			

Table 12: Results of multifactor ANOVA of joint damage excluding the open pit area.

	Sum of squares	df	Mean square	F	p value
Intercept	7.84	1	7.84	9.333	0.038*
Falling point spacing	2.16	4	0.54	0.643	0.66
Angle of penetration surface	0.56	4	0.14	0.167	0.945
Fragment 1 angle	2.16	4	0.54	0.643	0.66
Fragment 2 angle	2.96	4	0.74	0.881	0.547
Speed combination	2.96	4	0.74	0.881	0.547
Residual	3.36	4	0.84		
		$R^2 = 0.763$			

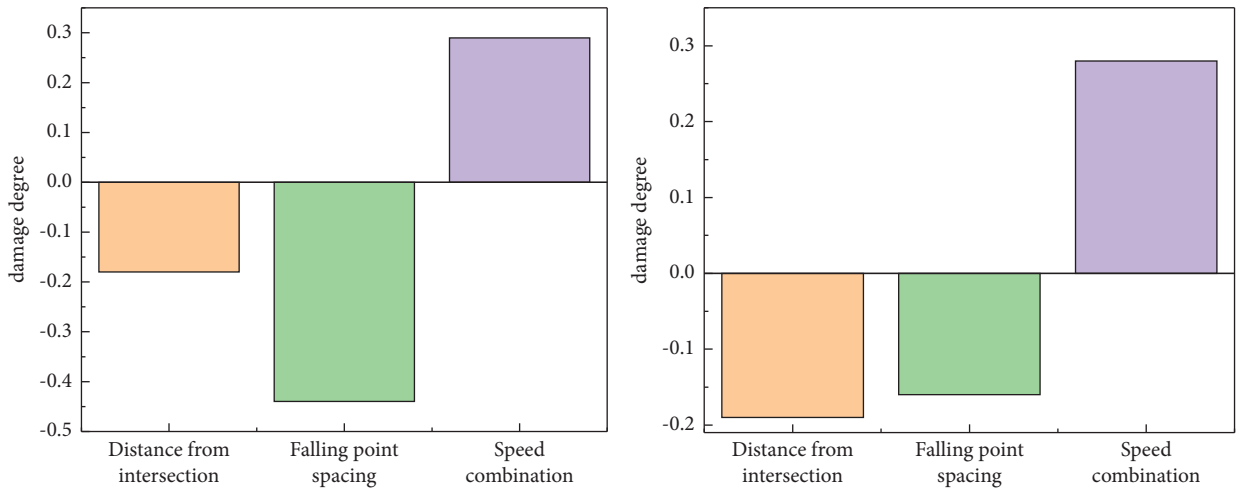

Figure 18: Standardized regression coefficients of optimized variables for two joint damage degrees.

Table 13: Comparison of coplanar and heterogeneous joint processes.

Time (ms)	Coplanar penetration	Different surface penetration
0.01	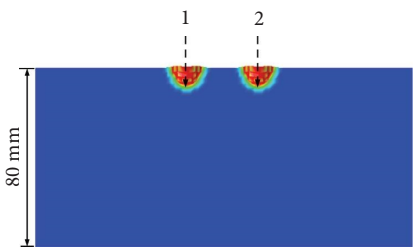	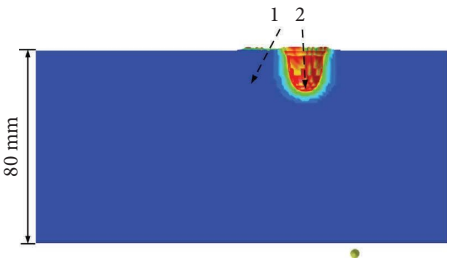

Table 13: Continued.

Time (ms)	Coplanar penetration	Different surface penetration
0.07	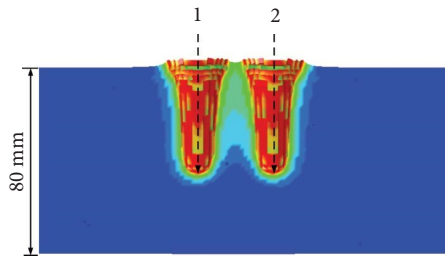	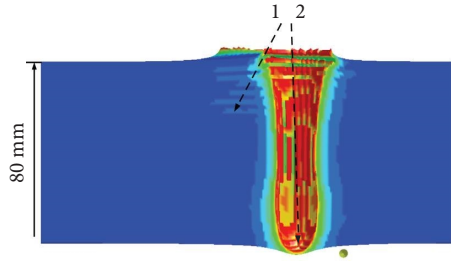
0.22	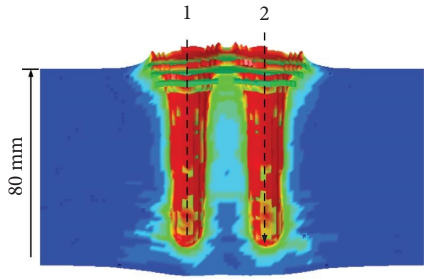	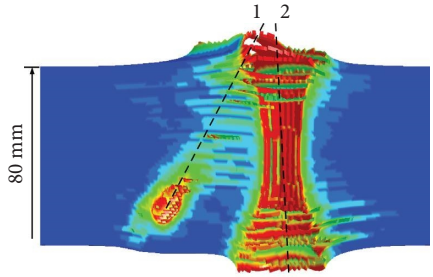
0.50	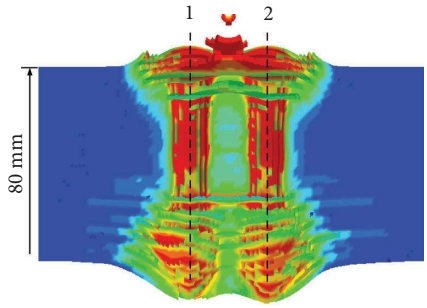	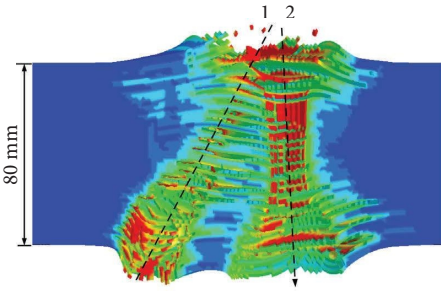

similar points or near the concrete area where the fragment tracks intersect, so as to reduce the damage degree of concrete under different planes.

As shown in Table 13, the process of fragment penetrating concrete is analyzed from the cloud image of joint damage. The joint response process of fragment penetration is observed by comparing the coplanar and the different planes. The coplanar penetration basically acts on the concrete target in the same time and space, so that the joint action process is continuous. Due to the different combinations of inclination angle and velocity and the inconsistent distance in space, there are various forms of space-time superposition in the joint action area, so that the joint form is mostly the destruction of a single area.

From the perspective of joint damage forms caused by different types of processes, the increase of variables between fragments on different sides makes it difficult to combine fragments even if 3/4 of the fragments have less intersection in the simulation. According to the results of the coplanar and nonplanar analysis, the speed and angle are the common factors that affect the damage size of the two fragments. The joint damage is affected by the initial distance between the two fragments and the distance from the intersection line of the penetration surface, that is, the smaller the two distances, the greater the joint damage degree between the fragments.

By analyzing and comparing the joint damage forms of the two regions, it can be seen that the joint damage degree of the open pit area and the collapse area is larger when they are coplanar, and the fragments of the tunnel area of both are relatively small, but the damage degree of the tunnel area of different planes is greater than that of coplanar penetration under some conditions.

3. Conclusions

Based on the research on the damage of a single fragment to three areas of concrete (impact the front face, impact the back face, and tunnel area) through direct and oblique penetration, the mechanism and form of joint damage can be seen by comparing the differences between coplanar and nonplanar joint damage between fragments. In the study of the joint damage of finite thickness concrete, through the data analysis of the occurrence time, damage form, and damage degree of the joint damage, the following conclusions are obtained:

(1) Coplanar joint damage is relatively regular. The main factor affecting the occurrence and degree of joint damage is fragment spacing, followed by velocity. The smaller the fragment spacing and the faster the speed, the greater the degree of joint damage. The PLS regression coefficients of the surface joint length

and the surface joint time of fragment spacing are 0.70 and 0.68, respectively.

(2) The damage mode of different surface damage is complex, in which the distance between the impact points mainly affects the damage degree of the pit opening area, and its PLS regression coefficient is 0.44 (the intersection distance is 0.18 at this time). The damage degree of the collapse area is affected by the intersection distance between the flying-out point on the back of the two and the penetration surface. The probability of joint damage in the tunnel area is the smallest. The damage on the different surfaces mostly occurs near the two falling points of the concrete and the area at the intersection of the trajectory. The regression coefficient of the intersection distance is 0.19 (the distance between the falling points is 0.16 at this time).

(3) The scoring of joint damage degree is closely related to each fragment variable, reflecting the joint degree between the two fragments. The occurrence of various types of joint damage can be explained by the parameters between the two fragments, which can be extended to the damage research of the warhead as a whole.

Data Availability

The data used to support the findings of the study can be obtained from the corresponding author upon request. The data are not publicly available due to programming privacy in structural design.

Conflicts of Interest

The authors declare that they have no conflicts of interest.

Acknowledgments

This research was funded by the Basic Research Plan of Shanxi Province in 2021 (free exploration) (Grant no. 20210302123207) and 2021 Shanxi Graduate Innovation Project (Grant no. Y2021576).

References

[1] J. P. Yin and Z. J. Wang, *Ammunition*, Beijing University of Technology Press, Beijing, China, 2017.

[2] C. Heckotter and A. Vepsa, "Experimental investigation and numerical analyses of reinforced concrete structures subjected to external missile impact," *Progress in Nuclear Energy*, vol. 84, pp. 56–67, 2015.

[3] L. L. He, X. W. Chen, and X. A. He, "Parametric study on mass loss of penetrators," *Acta Mechanica Sinica*, vol. 26, no. 4, pp. 585–597, 2010.

[4] Y. C. Shi, J. Wang, and J. Cui, "Experimental studies on fragments of reinforced concrete slabs under close-in explosions," *International Journal of Impact Engineering*, vol. 144, Article ID 103630, 2020.

[5] H. J. Wu, S. Zhang, and F. L. Huang, "Research progress in penetration/perforation into reinforced concrete targets," *Acta Armamentarii*, vol. 39, pp. 182–208, 2018.

[6] A. A. Konyaev, V. F. Tolkachev, and T. M. Platova, "Experimental testing of the fracture of concrete and re-inforced concrete plates under impact," *Journal of Applied Mechanics and Technical Physics*, vol. 56, no. 6, pp. 1031–1037, 2015.

[7] S. Lee, G. Kim, H. Kim, M. Son, G. Choe, and J. Nam, "Strain behavior of concrete panels subjected to different nose shapes of projectile impact," *Materials*, vol. 11, no. 3, p. 409, 2018.

[8] C. Liu, X. F. Zhang, H. H. Chen, J. P. Wang, H. Y. Wei, and W. Xiong, "Experimental and theoretical study on steel long-rod projectile penetration into concrete targets with elevated impact velocities," *International Journal of Impact Engineering*, vol. 138, Article ID 103482, 2020.

[9] S. M. Zakir, Y. L. Li, and T. Suo, "Numerical prediction of projectile residual velocity after penetration of reinforced concrete with different reinforcing bar arrangements," *Materials Research Innovations*, vol. 15, no. 1, pp. 191–194, 2011.

[10] Y. Cheng, J. Liu, X. F. Liu, S. B. Jin, and Y. Zhang, "Theoretical and numerical analysis on anti-penetration property of reinforced concrete target under normal penetration," *Science Technology and Engineering*, vol. 19, pp. 97–103, 2019.

[11] Y. J. Deng and X. W. Chen, "Experimental and numerical study on normal penetration of a projectile into a reinforced concrete target," *Explosion and impact*, vol. 40, pp. 26–36, 2020.

[12] Y. Liu, C. M. Song, Y. Huang, and B. Liu, "Experimental and analysis on oblique penetration of projectiles into reinforced concrete target," *Journal of PLA University of Technology*, vol. 14, pp. 64–68, 2013.

[13] L. Shen, S. Q. Gao, and L. Jin, "Numerical simulation of projectile oblique penetration into concrete," *Journal of Rockets and Guidance*, vol. 32, pp. 61–64, 2012.

[14] J. Duan, K. H. Wang, and G. Zhou, "Critical ricochet performance of penetrator impacting concrete targets," *Explosion and impact*, vol. 36, pp. 797–802, 2016.

[15] G. Zhou and M. R. Li, "Mechanism on hypervelocity penetration of a tungsten alloy projectile into a concrete target," *Explosion and impact*, vol. 41, pp. 93–106, 2021.

[16] J. W. Liu, X. F. Zhang, and C. Li, "Study on mass erosion model of projectile penetrating concrete at high speed considering variation of friction coefficient," *Explosion and impact*, vol. 41, pp. 114–124, 2021.

[17] Y. Q. Lv, N. X. Chen, and H. J. Wu, "Mechanism of high-velocity projectile penetrating into ultrahigh performance concrete target," *Acta Armamentarii*, vol. 43, pp. 37–47, 2022.

[18] C. Z. Wang, A. J. Chen, Z. Q. Li, C. A. Gong, S. Wang, and W. M. Yan, "Experimental and numerical investigation on penetration of clay masonry by small high-speed projectile," *Defence Technology*, vol. 17, no. 4, pp. 1514–1530, 2021.

[19] C. Sauer, A. Heine, and W. Riedel, "Developing a validated hydrocode model for adobe under impact loading," *International Journal of Impact Engineering*, vol. 104, pp. 164–176, 2017.

[20] L. Y. Xu, F. Cai, Y. Y. Xue, C. Takahashi, and Y. Y. Li, "Numerical analyses of local damage of concrete slabs by normal impact of deformable solid projectiles," *KSCE Journal of Civil Engineering*, vol. 23, no. 12, pp. 5121–5132, 2019.

[21] S. C. Lin and J. Cui, "Basic characteristics of high-speed fragments upon perforation of reinforced concrete slab," *Journal of Performance of Constructed Facilities*, vol. 34, no. 6, 2020.